

Magnetic structures and excitations in CePd₂(Al,Ga)₂ series: Development of the “vibron” statesM. Klicpera,^{1,2,*} M. Boehm,² P. Doležal,¹ H. Mutka,² M. M. Koza,² S. Rols,² D. T. Adroja,^{3,4} I. Puente Orench,^{2,5} J. Rodríguez-Carvajal,² and P. Javorský¹¹Charles University, Faculty of Mathematics and Physics, Department of Condensed Matter Physics, Ke Karlovu 5, 121 16 Prague 2, Czech Republic²Institut Laue-Langevin, 71 avenue des Martyrs, CS 20156, 38042 Grenoble Cedex 9, France³ISIS Facility, Rutherford Appleton Laboratory, Chilton, Didcot, Oxon OX11 0QX, United Kingdom⁴Highly Correlated Matter Research Group, Physics Department, University of Johannesburg, PO Box 524, Auckland Park 2006, South Africa⁵Instituto de Ciencia de Materiales de Aragón, CSIC, Pedro Cerbuna 12, 50009 Zaragoza, Spain

(Received 26 February 2016; revised manuscript received 10 January 2017; published 3 February 2017)

CePd₂Al_{2-x}Ga_x compounds crystallizing in the tetragonal CaBe₂Ge₂-type structure (space group *P4/nmm*) and undergoing a structural phase transition to an orthorhombic structure (*Cmme*) at low temperatures were studied by means of neutron scattering. The amplitude-modulated magnetic structure of CePd₂Al₂ is described by an incommensurate propagation vector $\vec{k} = (\delta_x, \frac{1}{2} + \delta_y, 0)$ with $\delta_x = 0.06$ and $\delta_y = 0.04$. The magnetic moments order antiferromagnetically within the *ab* planes stacked along the *c* axis and are arranged along the direction close to the orthorhombic *a* axis with a maximum value of 1.5(1) μ_B/Ce^{3+} . CePd₂Ga₂ reveals a magnetic structure composed of two components: the first is described by the propagation vector $\vec{k}_1 = (\frac{1}{2}, \frac{1}{2}, 0)$, and the second one propagates with $\vec{k}_2 = (0, \frac{1}{2}, 0)$. The magnetic moments of both components are aligned along the same direction—the orthorhombic [100] direction—and their total amplitude varies depending on the mutual phase of magnetic moment components on each Ce site. The propagation vectors \vec{k}_1 and \vec{k}_2 describe also the magnetic structure of substituted CePd₂Al_{2-x}Ga_x compounds, except the one with *x* = 0.1. CePd₂Al_{1.9}Ga_{0.1} with magnetic structure described by \vec{k} and \vec{k}_1 stays on the border between pure CePd₂Al₂ and the rest of the series. Determined magnetic structures are compared with other Ce 112 compounds. Inelastic neutron scattering experiments disclosed three nondispersive magnetic excitations in the paramagnetic state of CePd₂Al₂, while only two crystal field (CF) excitations are expected from the splitting of ground state $J = \frac{5}{2}$ of the Ce³⁺ ion in a tetragonal/orthorhombic point symmetry. Three magnetic excitations at 1.4, 7.8, and 15.9 meV are observed in the tetragonal phase of CePd₂Al₂. A structural phase transition to an orthorhombic structure shifts the first excitation up to 3.7 meV, while the other two excitations remain at almost the same energy. The presence of an additional magnetic peak is discussed and described within the Thalmeier-Fulde CF-phonon coupling (i.e., magnetoelastic coupling) model generalized to the tetragonal point symmetry. The second parent compound CePd₂Ga₂ does not display any sign of additional magnetic excitation. The expected two CF excitations were observed. The development of magnetic excitations in the CePd₂Al_{2-x}Ga_x series is discussed and crystal field parameters determined.

DOI: [10.1103/PhysRevB.95.085107](https://doi.org/10.1103/PhysRevB.95.085107)**I. INTRODUCTION**

The tetragonal CeT₂X₂ ternaries (where *T* = transition metal *d* element and *X* = *p* metal) form a large family of compounds with often unique physical properties. CeCu₂Si₂ exhibits an unstable 4*f* shell and a transition into a superconducting state in the vicinity of a quantum critical point (QCP) [1–3]. Pressure-induced superconductivity is observed, e.g., in CePd₂Si₂ [4], CeRh₂Si₂ [5], or CeCu₂Ge₂ [6]. CePd₂Si₂ and CeRh₂Si₂ show weak valence fluctuations which become stronger with increasing pressure. At high pressures a rapid transition from the Kondo regime into the valence fluctuation regime is observed, while the superconductivity does not seem to be directly influenced [7]. A valence fluctuating state at ambient pressure is also observed, e.g., in CeNi₂Si₂ or CeCo₂Si₂ [8,9]. The localized 4*f* electrons are strongly influenced by crystal field (CF) and long-range RKKY interaction and are often screened by conduction electrons. In addition, electron-phonon interaction has been proposed in

CePd₂Al₂ leading to a formation of a new quantum quasibound state [13]. Besides CePd₂Al₂, this so called vibron state has been proposed for only two other Ce-based compounds: CeAl₂ [10–12] and CeCuAl₃ [14], further for PrNi₂ [15], and quite recently for pyrochlore Tb₂Ti₂O₇ [16,17]. An additional magnetic peak in the energy spectra could be described within the Thalmeier-Fulde model [11], first proposed for cubic CeAl₂. The model features a strong magnetoelastic coupling between orbital and lattice degrees of freedom leading to a new type of magnetophonon mode and to changes of macroscopic properties [11,14]. Moreover, a significant number of CeT₂X₂ compounds undergo a structural phase transition from tetragonal to a lower symmetry structures (or structural distortion), e.g., CeNi₂Sn₂ [18], CePt₂Sn₂ [18], CeRh₂Sb₂ [19], CePt₂Ge₂ [20], or CePd₂Ga₂ [21,22].

The present study focuses on the CePd₂Al₂ compound, so far the first member of the CeT₂X₂ family exhibiting an additional peak in the CF spectrum [13], which cannot be explained by the standard analysis based on symmetry arguments of the local environment around the Ce atom. We further investigated the influence of Ga substitution on the spectra by means of neutron scattering techniques.

*mi.klicpera@seznam.cz

CePd₂Al₂ crystallizes in the CaBe₂Ge₂-type tetragonal structure (*P4/nmm*, 129) and undergoes a phase transition to the orthorhombic *Cmme* structure at around $T_{\text{struc}}^{\text{CePd}_2\text{Al}_2} = 13$ K [13,23–25] (see Fig. 1 for illustration). An antiferromagnetic order below $T_N^{\text{CePd}_2\text{Al}_2} = 2.7$ K and field-induced metamagnetic transitions around 2 T and 4 T for the crystallographic [100] and [001] directions are observed, respectively [24]. The nonmagnetic LaPd₂Al₂ undergoes the same type of structural phase transition as its Ce counterpart ($T_{\text{struc}}^{\text{LaPd}_2\text{Al}_2} = 91.5$ K) [13] excluding a magnetoelastic origin of the phase transition. Furthermore it becomes superconducting below 1.8 K [26]. (Ce,La)Pd₂Ga₂ compounds reveal identical structural phase transition to those of their Al counterparts ($T_{\text{struc}}^{\text{CePd}_2\text{Ga}_2} = 127$ K, $T_{\text{struc}}^{\text{LaPd}_2\text{Ga}_2} = 64.1$ K) as well as the antiferromagnetic ground state (below 2.2 K) and superconducting state (below 2 K), respectively [21–23,26]. In contrast with *RPd₂Al₂*, where structural transition temperatures in the Ce- and La-based compounds show $T_{\text{struc}}^{\text{CePd}_2\text{Al}_2} < T_{\text{struc}}^{\text{LaPd}_2\text{Al}_2}$, *RPd₂Ga₂* compounds reveal the opposite: $T_{\text{struc}}^{\text{CePd}_2\text{Ga}_2} > T_{\text{struc}}^{\text{LaPd}_2\text{Ga}_2}$ [21,23]. Such an observation was tentatively attributed to the occurrence of the vibron state in CePd₂Al₂ which stabilizes the tetragonal structure [13]. Following the concentration dependence of structural transition temperatures in *RPd₂Al_{2-x}Ga_x* compounds [23], one can assume the following scenario: the strong CF excitation-phonon interaction takes place in compounds with $x < 0.8$, where $T_{\text{struc}}^{\text{Ce}} < T_{\text{struc}}^{\text{La}}$, the strength of interaction decreases in the concentration interval $x \in (0.8, 1.2)$, and for $x > 1.2$ (where $T_{\text{struc}}^{\text{Ce}} > T_{\text{struc}}^{\text{La}}$) there are no vibrons. The aim of the present investigation of the CePd₂(Al,Ga)₂ series by inelastic neutron scattering is to confirm this scenario.

II. EXPERIMENTAL

Polycrystalline samples (mass ≈ 18 g) from the (Ce,La)Pd₂Al_{2-x}Ga_x series, where $x = 0.0, 0.1, 0.4, 0.8, 1.2$ and 2.0, were prepared by the arc-melting of pure elements (2N8 for Ce, 3N for La, 4N5 for Pd, 6N for Al, and 7N for Ga, where 2N8 means 99.8% metals basis, Alfa Aesar

under protective argon atmosphere. 0.5% (of mass) of Ga was added to account for significantly higher evaporation of Ga compared to other constituent elements. The samples were turned and remelted several times to ensure their homogeneity. As-cast samples were additionally sealed in a quartz glass under pressure of 10^{-4} Pa and annealed at 800 °C for 10 days to further improve their homogeneity.

The room temperature crystal structure of prepared samples and their phase purity were checked by powder x-ray diffraction and energy-dispersive x-ray analysis (EDX), respectively. Traces of a small amount of unknown impurity phase were detected by EDX. The x-ray analysis confirmed the samples crystallizing in the tetragonal CaBe₂Ge₂-type structure. The refined lattice parameters (FullProf program [27]) were identical within the experimental error to previously published data [23]. The time relaxation method and physical property measurement system (PPMS; Quantum Design) were used for the specific-heat measurement on samples with mass of ≈ 20 mg.

The powder neutron diffraction experiments on CePd₂Al₂ and CePd₂Ga₂ were done at the Institut Laue-Langevin (ILL). Thermal neutron diffraction was carried out between 1.5 and 100 K using a monochromatic beam of 2.52 Å at the high-flux powder diffractometer D1B equipped with a high-efficiency position-sensitive detector which collects patterns of 128° in 2θ . The inelastic neutron scattering experiments were performed in the temperature interval (1.5, 120/140) K on the time-of-flight spectrometers IN6 (low-energy part of the spectra, for the excitations expected at around 1.5 meV) and IN4 (higher-energy part of the spectra) also at the ILL. The measurements were carried out using the incident neutron energies 3.15 meV and 4.77 meV (IN6), 16.56 meV, 28.31 meV and 36.36 meV (IN4). The powder samples were loaded inside aluminum cells of dimensions $4 \times 3 \times 0.4$ cm. The cells were placed inside cadmium frames to reduce background. The experimental conditions were chosen for the best resolution at the elastic position giving respective resolutions 0.08 meV (IN6), 1.0, 1.6 and 2.2 meV (IN4). Auxiliary measurements of an empty can and vanadium for calibration purposes were

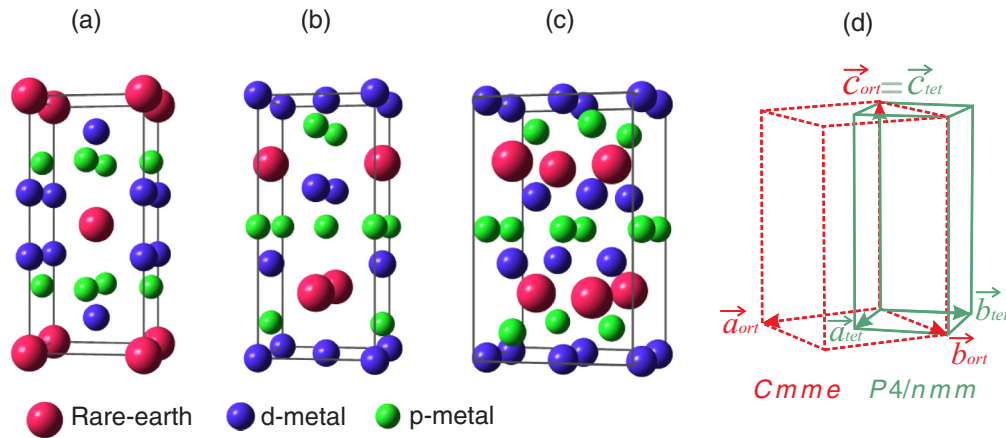


FIG. 1. (a) Tetragonal crystal structure of ThCr₂Si₂-type (space group *I4/mmm*, 139). (b) Tetragonal CaBe₂Ge₂-type structure (space group *P4/nmm*, 129), high-*T* phase of investigated compounds. (c) Orthorhombic structure (space group *Cmme*, 67), low-*T* phase of investigated compounds. (d) Unit cells of orthorhombic *Cmme* and tetragonal *P4/nmm* space groups with special set of orthorhombic parameters $a_{\text{orthorhombic}} = b_{\text{orthorhombic}} = \sqrt{2}a_{\text{tetragonal-CaBe}_2\text{Ge}_2}$ allowing the description of the tetragonal structure (*P4/nmm*) by *Cmme* space group.

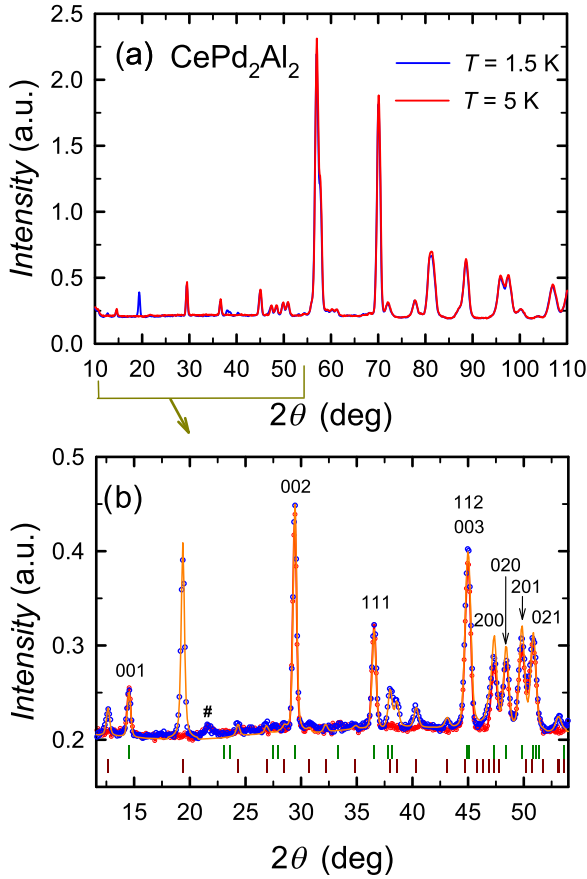


FIG. 2. (a) Powder neutron diffraction patterns of CePd_2Al_2 taken at 1.5 K and 5 K; see text for details. Panel (b) highlights the low-angle region. Full orange line represents the fit done with the FullProf program [27]. Tick marks denote the positions of nuclear (green) and magnetic [$\vec{k} = (0.06, 0.54, 0)$; dark red] Bragg reflections. Symbol # labels the peak of a foreign phase, which is not of magnetic origin.

carried out. Data were corrected for container scattering, absorption and self-shielding, detector efficiency variation, and energy dependence. The normalization to a vanadium standard allowed the calculation of the dynamic structure factor $S(Q, \omega)$ in absolute units. This basic data treatment was carried out with the software package LAMP [28,29]. The complete sets of the experimental data can be found in Refs. [30–32].

III. RESULTS AND DISCUSSION

A. Magnetic structures in CePd_2Al_2 and CePd_2Ga_2 : Neutron diffraction

1. Magnetic propagation vectors

Measured diffraction patterns of CePd_2Al_2 and CePd_2Ga_2 are plotted in Figs. 2 and 3, respectively. The low-temperature crystal structure of CePd_2Al_2 and CePd_2Ga_2 is of orthorhombic $Cmme$ type (see Fig. 1 for illustration) [22] with the following atomic positions:

$$\begin{aligned} 4\text{Ce in (4g): } & (0, \frac{1}{4}, z_{\text{Ce}}), \\ 4\text{Pd in (4a): } & (\frac{1}{4}, 0, 0), \\ 4\text{Pd in (4g): } & (0, \frac{1}{4}, z_{\text{Pd}}), \end{aligned}$$

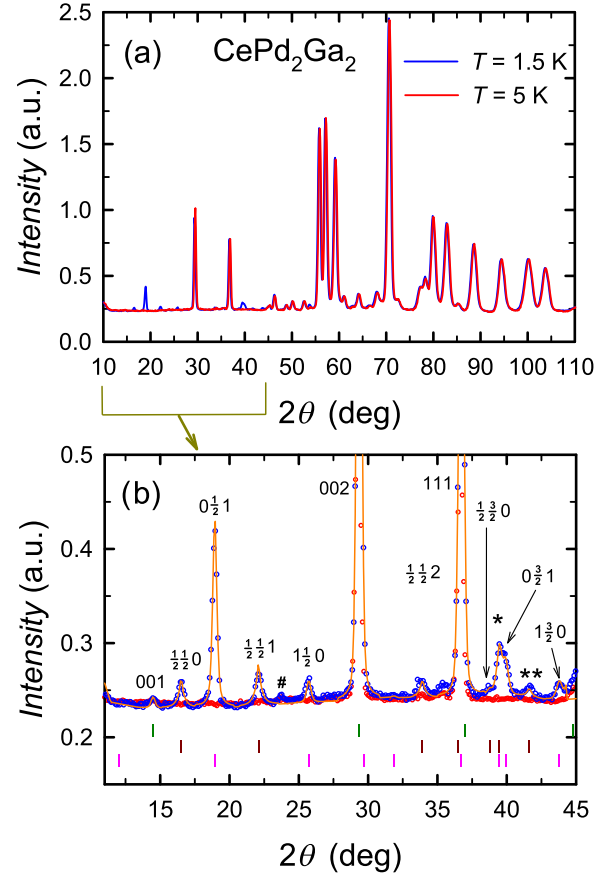


FIG. 3. (a) Powder neutron diffraction patterns of CePd_2Ga_2 taken at 1.5 K and 5 K. Panel (b) highlights the low-angle region. Full orange line represents the fit done with the FullProf program [27]. Tick marks denote the positions of nuclear (green) and magnetic Bragg reflections [dark red for $\vec{k}_1 = (\frac{1}{2}, \frac{1}{2}, 0)$ and pink for $\vec{k}_2 = (0, \frac{1}{2}, 0)$]. Symbol # labels the peak of a foreign phase, which is not of magnetic origin. All pronounced reflections are labeled; symbol * marks the peak bounded with magnetic reflections ($\frac{3}{2}, \frac{1}{2}, 1$) and ($1, \frac{1}{2}, 2$); symbol ** marks the magnetic reflection ($\frac{1}{2}, \frac{3}{2}, 1$).

$$4\text{Al(Ga) in (4b): } (\frac{1}{4}, 0, \frac{1}{2}),$$

$$4\text{Al(Ga) in (4g): } (0, \frac{1}{4}, z_{\text{Al(Ga)}}).$$

The structure parameters determined at $T = 5$ K for both CePd_2X_2 compounds are listed in Table I. A comparison of diffraction patterns taken in the paramagnetic and the ordered state (at temperatures 5 K and 1.5 K, respectively) reveals several (about ten) clear peaks of magnetic origin for each compound. We note that the most intense magnetic peak in the diffraction pattern of CePd_2Ga_2 corresponds to the magnetic reflection found in our former powder neutron diffraction experiment [23].

The present diffraction patterns allow an unambiguous determination of the magnetic propagation vectors, as well as the study of magnetic structures in both CePd_2X_2 compounds. The observed magnetic peaks in CePd_2Al_2 are described by the incommensurate propagation vector $\vec{k} = (\delta_x, \frac{1}{2} + \delta_y, 0)$ with $\delta_x = 0.06$ and $\delta_y = 0.04$, while two commensurate magnetic propagation vectors, $\vec{k}_1 = (\frac{1}{2}, \frac{1}{2}, 0)$ and $\vec{k}_2 = (0, \frac{1}{2}, 0)$ —together with $-\vec{k}_2$ ($\vec{k}_2 \neq -\vec{k}_2$)—are necessary to describe the magnetic structure of CePd_2Ga_2 . The positions of magnetic reflections

TABLE I. Lattice parameters and fractional atomic positions of CePd_2Al_2 and CePd_2Ga_2 compounds as determined from neutron diffraction data measured at 5 K. The temperatures of structural (T_{struc}) and magnetic (T_{N}) phase transitions were determined from specific-heat measurement. Propagation vectors, maximum value of magnetic moment on Ce site, and its direction as determined from neutron diffraction (measured below 2 K) are included as well. The refinement of nuclear and magnetic structures was done within the $Cmme$ space group using the FullProf package [27]. R_{Bragg} and R_{M} stay for agreement factors between measured data and fits for nuclear and magnetic structure, respectively. For the convenience the Wyckoff positions for individual atoms are listed.

	CePd_2Al_2	CePd_2Ga_2	
a (Å)	6.268(2)	6.401(2)	Wyckoff atomic positions in orthorhombic $Cmme$:
b (Å)	6.132(2)	5.943(2)	
c (Å)	9.886(3)	9.905(4)	4Ce in (4g): $(0, \frac{1}{4}, z_{\text{Ce}})$
z_{Ce}	0.756(3)	0.75(1)	4Pd in (4a): $(\frac{1}{4}, 0, 0)$
z_{Pd}	0.371(2)	0.372(7)	4Pd in (4g): $(0, \frac{1}{4}, z_{\text{Pd}})$
$z_{\text{Al(Ga)}}$	0.119(3)	0.124(6)	4Al(Ga) in (4b): $(\frac{1}{4}, 0, \frac{1}{2})$
T_{struc} (K)	13.0(2)	127(3)	4Al(Ga) in (4g): $(0, \frac{1}{4}, z_{\text{Al(Ga)}})$
R_{Bragg} (%)	2.8	5.3	
T_{N} (K)	2.7(1)	2.2(1)	
\vec{k}	(0.06, 0.54, 0)		
\vec{k}_1			$(\frac{1}{2}, \frac{1}{2}, 0)$
\vec{k}_2			$(0, \frac{1}{2}, 0)$
μ_{max} ($\mu_{\text{B}}/\text{Ce}^{3+}$)	1.47(4)	1.6(1)	
μ direction	$\approx \ a$	$\ a$	
R_{M} (%)	14.9	9.9	

are marked below the diffraction patterns presented in Figs. 2 and 3. We highlight that the identified $\vec{k}_2 = (0, \frac{1}{2}, 0)$, describing also the strongest magnetic reflection in CePd_2Ga_2 , corresponds well to the $(\frac{1}{4}, \frac{1}{4}, 0)$ propagation vector in the triclinic description; i.e., our recent and former [23] diffraction studies are fully consistent. (The triclinic low- T crystal structure was previously determined by Kitagawa *et al.* [21] and our former diffraction data [23] did not allow us to determine higher symmetrical crystal structure.) The orthorhombic $Cmme$ structure was determined as the low- T crystal structure of CePd_2Ga_2 [and all $\text{CePd}_2(\text{Al}, \text{Ga})_2$] quite recently. The study of low-temperature crystal structures in this system will be published separately [22].

The determined magnetic propagation vectors and known structure parameters allow us to calculate the possible magnetic structures by performing a thorough symmetry analysis employing the programs BasIreps [27] and MaxMagn [33]. The details on maximal magnetic subgroups analysis are presented in the Appendix.

2. Magnetic structure of CePd_2Al_2

The incommensurate magnetic structure of CePd_2Al_2 is described by a refined propagation vector $\vec{k} = (0.058(2), 0.5370(7), 0)$. We have assumed a single- \vec{k} (pair: $\vec{k}, -\vec{k}$) amplitude-modulated magnetic structure (spiral or cycloidal structures give worse results). The representation analysis using BasIreps [27] provides in this case the full description of the magnetic structure. There are two irreducible representations (irreps) of the propagation vector group $G_{\vec{k}} = C11b$

(monoclinic in a nonstandard setting), labeled as $\Gamma_1(1, \alpha)$ and $\Gamma_2(1, -\alpha)$, with $\alpha = 0.11629 - 0.99322i$. The first component refers to the character of the identity operator $1 = (x, y, z)$ and the second component to the character of the operator $b = (x, y + 1/2, -z)$. The experimental data are perfectly refined using the irrep Γ_2 that gives the following Fourier coefficients for the atoms in the primitive cell: $\text{Ce}_1 = (x, y, z), \vec{S}_1 = \frac{1}{2}(u, v, w)$ and $\text{Ce}_2 = (x, y + 1/2, -z + 1), \vec{S}_2 = \frac{1}{2}(u, v, -w) \exp(-2\pi i \{-0.23145\})$. The coefficients (u, v, w) may be, in general, complex (giving rise to spiral or cycloidal structures); however taking them as real numbers we obtain an amplitude-modulated structure with refined values: $u = 1.38(3), v = 0.1(1), w = 0.50(6)$, corresponding to the maximum amplitude of $1.47(4)\mu_{\text{B}}/\text{Ce}^{3+}$. The agreement factor between the fit and magnetic data for this case is $R_{\text{M}} = 14.9\%$. Notice that the major component is along the a axis, but the component along the c axis is non-negligible. The maximum magnetic moment is significantly lower than the magnetic moment of the Ce^{3+} free ion, which is quite consistent with the expected reduction of magnetic moment due to the influence of the crystal field and it is fully coherent with our magnetic measurement [24]. The fit of the calculated magnetic structure to the measured data is presented in Fig. 2.

3. Magnetic structure of CePd_2Ga_2

Let us now discuss the case of CePd_2Ga_2 in which two propagation vectors are active. Considering the propagation vector \vec{k}_2 we obtain four one-dimensional irreps of $G_{\vec{k}} = Cm2_1b$, labeled as $\Gamma_1(1, i, -i, -1), \Gamma_2(1, i, i, 1), \Gamma_3(1, -i, -i, 1)$, and

$\Gamma_4(1, -i, i, -1)$; the orders of operators are $1, 2_{1y}, b_{xy},$ and m_{yz} . The measured magnetic peaks corresponding to k_2 are well described by $\Gamma_2(1, i, i, 1)$ which has Fourier coefficients for the two Ce atoms in the primitive cell $\vec{S}_1 = \frac{1}{2}(u, 0, 0)$ and $\vec{S}_2 = i\frac{1}{2}(u, 0, 0) = \exp(-2\pi i\{-0.25\})$; thus the moments are constrained along the a axis. For the propagation vector \vec{k}_1 we obtain a single two-dimensional irrep of $G_k = C112_1/b$. The basis vectors that are in a general direction of the representation space do not constrain the magnetic moments of the two sublattices; however we can select special directions corresponding to the two different magnetic space groups discussed above: monoclinic P_a2 and triclinic $P_5\bar{1}$. The superposition of the two propagation vectors reduces the symmetry to $P_5\bar{1}$ with the only restriction of having the atoms related by the center of symmetry to be parallel. We therefore selected the direction of the Fourier coefficients \vec{S}_{k_1} to be parallel to \vec{S}_{k_2} and pointing along the a axis, admitting the order according to the $\Gamma_2(1, i, i, 1)$ irrep.

As a consequence the magnetic moments belonging to each of the two components in CePd₂Ga₂ are aligned along one direction and order antiferromagnetically within planes stacked along the c axis. Compared to CePd₂Al₂, the tilt out of the a axis does not bring any significant improvement of the fit.

The value of the magnetic moment for the component described by the propagation vector \vec{k}_1 is $0.6(1) \mu_B/\text{Ce}^{3+}$. The maximum value of the magnetic moment for the second component (\vec{k}_2 propagation vector) is then $1.5(1) \mu_B/\text{Ce}^{3+}$. While the first component is fully determined ($\vec{k}_1 \equiv -\vec{k}_1$), the magnetic phase of the second component remains ambiguous ($\vec{k}_2 \in \text{IBZ}$: interior of the Brillouin zone). In the case of a multiple-non-symmetry-related- \vec{k} magnetic structure, it is not possible to determine the magnetic moments configuration unambiguously, unless a strong magnetoelastic coupling is present. The phase between the different Fourier components of the magnetic moments cannot be determined by diffraction methods. There exist infinitely many structures being able to explain the measured diffraction patterns. Thus, diffraction alone is unable to provide a unique solution. Symmetry constraints and, more importantly, restrictions on the amplitude of the magnetic moments can reduce the number of solutions [34]. The magnetic structure of CePd₂Ga₂ described by the two commensurate propagation vectors thus cannot be determined unambiguously.

The maximal value of the total magnetic moment on the Ce atom, which is the sum of the two components, is restricted by the value of the magnetic moment of the Ce³⁺ free ion ($2.14 \mu_B$). Such a limitation would play an important role in a choice of the magnetic phase of the second component of the magnetic moment, as the magnetic moments of the first component have a constant value. However, the sum of the magnetic moment values of both components is still slightly lower than the upper limit, even taking a zero phase shift between the components into account. Therefore, the phase shift between both components is arbitrary. The zero phase shift leads to total magnetic moments varying among 2, 0.9, and $0.6 \mu_B/\text{Ce}^{3+}$. In the case of a 45° shift, the total value of the magnetic moment varies between 1.6 and $0.4 \mu_B/\text{Ce}^{3+}$ depending only on the mutual sign of both magnetic components. The agreement factor between the fit and magnetic data

for all possible phase shifts remains the same, i.e., $R_M = 9.9\%$. Taking into account the reduced magnetic moment in the case of CePd₂Al₂, we tend to the 45° phase shift in CePd₂Ga₂ assuming also a reduced magnetic moment in this counterpart. Such a reduction is well in agreement with our magnetization measurement (the measured dependencies for both CePd₂X₂ compounds exhibit similar behavior) [23].

4. Discussion: Magnetic structures in CeT₂X₂ compounds

Let us briefly discuss the magnetic structures and their propagation vectors in other CeT₂X₂ compounds, although the magnetic structure is known only in a handful of them, and although most of these compounds crystallize in the tetragonal ThCr₂Si₂-type structure (space group $I4/mmm$, 139); see Fig. 1. The magnetic structure in CePd₂X₂ with $X = \text{Si}$ [35], Ge [36,37] consists of magnetic moments arranged along the [110] tetragonal direction and is described by the propagation vector $(\frac{1}{2}, \frac{1}{2}, 0)$. The same \vec{k} describes the magnetic structure in CeRh₂Si₂, but the magnetic moments point along the c axis and, moreover, a second component with a $(\frac{1}{2}, \frac{1}{2}, \frac{1}{2})$ propagation vector is present [38]. Both components point along [001] leading to a stacking of AFM planes with the total magnetic moment on Ce oscillating between the sum and difference values of these two components [38], similarly to the present case of CePd₂Ga₂. Ferromagnetic planes stacked antiferromagnetically along the c axis with magnetic moments aligned also along the c axis are found in CeAu₂Si₂ [38], CeRu₂Ge₂ [39] and CeAg₂Si₂ [38] exhibit magnetic moments parallel to the tetragonal a axis described by $\vec{k} = (k_x, 0, 0)$. CeCu₂Ge₂ with $\vec{k} = (0.28, 0.28, 0.54)$ and a spiral magnetic structure concludes our short list [40]. The magnetic structures in CePd₂Al₂ and CePd₂Ga₂ could be compared to the previous ones only after transformation from the orthorhombic to the tetragonal description (see Fig. 1 for illustration), i.e., $\vec{k}_1 = (\frac{1}{2}, \frac{1}{2}, 0) \rightarrow (\approx 0, \approx \frac{1}{2}, 0)^{\text{tetragonal}}$ and $\vec{k}_2 = (0, \frac{1}{2}, 0) \rightarrow (\approx \frac{1}{4}, \approx \frac{1}{4}, 0)^{\text{tetragonal}}$, and the crystallographic direction $[100]^{\text{orthorhombic}} \rightarrow \approx [110]^{\text{tetragonal}}$. By comparison of recently determined magnetic structures to other CeT₂X₂, we can conclude that all Pd-based compounds ($X = \text{Al, Ga, Si}$ [35], and Ge [36,37]) reveal the magnetic structure described by $\vec{k}^{\text{tetragonal}} = (k_x \neq 0, k_y \approx k_x, 0)$ and with magnetic moments aligned along $[110]^{\text{tetragonal}}$ or very close to this direction. Nevertheless, the magnetic structure of CePd₂Ga₂ is described by two propagation vectors and the propagation vector of CePd₂Al₂ is incommensurate. A systematic behavior of the propagation of magnetic moments in these compounds is not obvious so far. Nevertheless, the lattice parameters (i.e., the Ce-Ce interatomic distances) could play an important role in the magnetic structure formation. The c/a ratio seems to be a driving parameter as $c/a^{\text{tetragonal}} < 2.35$ for CePd₂X₂ [35–37], while $c/a^{\text{tetragonal}} > 2.35$ for other CeT₂X₂ compounds with different type of propagation and/or arrangement of magnetic moments.

B. Inelastic neutron scattering study on CePd₂(Al, Ga)₂ compounds

1. Magnetic Bragg reflections in elastic parts of measured CePd₂(Al, Ga)₂ spectra

The inelastic neutron scattering experiments performed on CePd₂(Al, Ga)₂ compounds using the IN6 and IN4

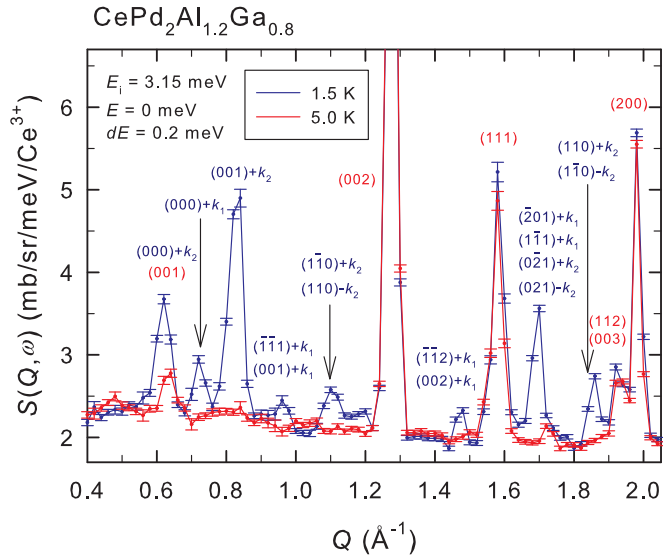


FIG. 4. Elastic part of $\text{CePd}_2\text{Al}_{1.2}\text{Ga}_{0.8}$ spectra (constant E cuts around center value $E = 0$ in intervals of 0.2 meV) measured using IN6 spectrometer at 1.5 K and 5 K, i.e., below and above magnetic ordering temperature, respectively. Nuclear and magnetic peaks are described; red and blue colors are used for better lucidity. The same notation of propagation vectors as in Sec. III A is used.

spectrometers disclose a significant number of microscopic properties of this system. Before proceeding to the pure inelastic scattering results, let us discuss the development of magnetic structure in the $\text{CePd}_2(\text{Al,Ga})_2$ series based on the elastic part of the E - Q maps measured employing the IN6 spectrometer. The constant E cuts were done around the center value $E = 0$ in intervals of 0.2 meV on data measured at 1.5 K and 5 K, i.e., below and above the magnetic ordering temperature. Besides (up to 7, depending on used energy range) nuclear Bragg reflections, the data measured at

1.5 K disclose several (up to 8 according to the compound and used energy of incoming neutrons) pure magnetic peaks. The energy cuts are shown for $\text{CePd}_2\text{Al}_{1.2}\text{Ga}_{0.8}$ in Fig. 4 as an example. Magnetic peaks in parent compounds (CePd_2Al_2 and CePd_2Ga_2) are clearly described, as expected, by propagation vectors determined on the basis of our neutron diffraction experiment on the D1B diffractometer (see previous part). The magnetic peaks in $\text{CePd}_2(\text{Al,Ga})_2$ with $x \geq 0.4$ are described by propagation vectors \vec{k}_1 and \vec{k}_2 as in the case of CePd_2Ga_2 . Nevertheless, the intensity on magnetic peaks differs significantly depending on Al-Ga concentration. The magnetic structure in substituted compounds is presumably similar to the one of CePd_2Ga_2 ; however it cannot be refined precisely based on measured data. $\text{CePd}_2\text{Al}_{1.9}\text{Ga}_{0.1}$ with magnetic structure described by \vec{k} seems to be close to the parent CePd_2Al_2 . However, we observe two weak magnetic peaks that cannot be described by \vec{k} but are described rather by \vec{k}_1 . $\text{CePd}_2\text{Al}_{1.9}\text{Ga}_{0.1}$ thus stays on the border between two types of magnetic structures represented by magnetic structures of CePd_2Al_2 and CePd_2Ga_2 .

We note that the magnetic moment arrangement in CePd_2Al_2 described by the incommensurate magnetic propagation vector \vec{k} is quite easily disrupted by Al-Ga substitution and transforms itself into a two (magnetic moments) components structure described by \vec{k}_1 and \vec{k}_2 . The magnetic structure in CePd_2Al_2 represents one of the fragile balanced structures and we can, to some extent, anticipate a relatively fast change of magnetic structure also with a substitution on Ce and Pd sites.

2. Magnetic excitations in CePd_2Al_2

The inelastic scattering experiments revealed three clear magnetic excitations in the energy spectrum of CePd_2Al_2 . These excitations are observed at 1.4, 7.8, and 15.9 meV in the tetragonal structure of CePd_2Al_2 (i.e., above 13 K)

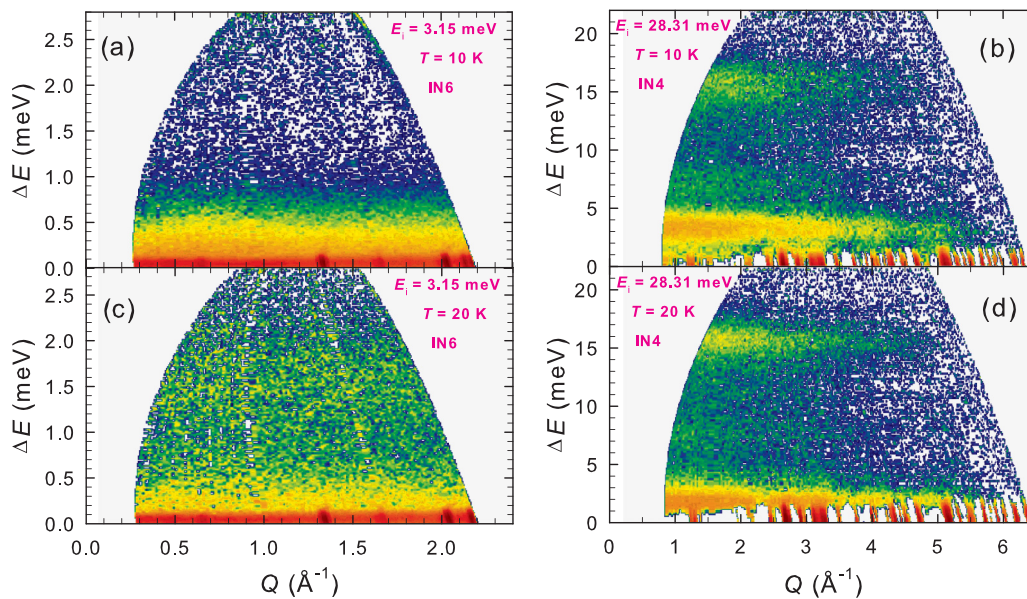


FIG. 5. Inelastic neutron scattering data measured on CePd_2Al_2 . Panels (a) and (b) show the measurements at 10 K (i.e., in the orthorhombic phase); panels (c) and (d) show the spectra determined at 20 K (i.e., in the tetragonal phase). Data in panels (b) and (d) highlight the magnetic scattering estimated by subtracting the data of the nonmagnetic LaPd_2Al_2 .

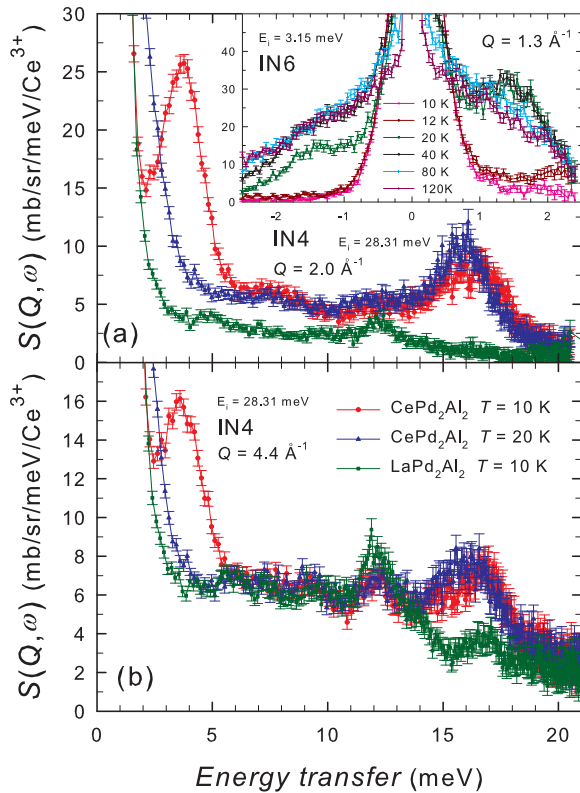


FIG. 6. Dynamic structure factor $S(Q, \omega)$ of CePd_2Al_2 and LaPd_2Al_2 at low (a) and high (b) momentum transfer Q (the constant Q cuts were done around center value Q in intervals of 1 and 0.5 \AA^{-1} for IN6 and IN4 measurements, respectively). The data measured in orthorhombic (10 K) and tetragonal (20 K) phases for CePd_2Al_2 are shown; LaPd_2Al_2 adopts the orthorhombic structure at temperatures lower than 91.5 K [13]. The inset contains the temperature evolution of the peak at 1.4 meV . Peak at -1.4 meV is a consequence of the principle of detailed balance.

and at $3.7, 7.8$ and 16 meV in the orthorhombic phase below 13 K (Fig. 5). The magnetic origin of these peaks is confirmed by a comparison with LaPd_2Al_2 data and by their Q and temperature dependencies. The data presented in Figs. 5(b) and 5(d) were obtained by subtracting a nonmagnetic analog data from CePd_2Al_2 via the relation

$S_M(\vec{Q}, \omega) = S^{\text{CePd}_2\text{Al}_2}(\vec{Q}, \omega) - \alpha S^{\text{LaPd}_2\text{Al}_2}(\vec{Q}, \omega)$, where α is the ratio of the total-scattering cross sections for RPd_2Al_2 with $R = \text{Ce}$ and La . The presence of the peak at around 1.4 meV energy transfer at 20 K in Fig. 5(c) is verified by the absence of such feature at 10 K [Fig. 5(a) and inset of Fig. 6] and by the observation of the same excitation in the vicinity of the elastic peak in IN4 data [Fig. 5(d)].

The spectra measured at different temperatures thus show that the structural phase transition from the tetragonal ($P4/nmm, 129$) to orthorhombic ($Cmme, 67$) structure (see Fig. 1 for illustration) has a strong impact on the energy diagram of CePd_2Al_2 . In particular, the first CF excitation moves from 1.4 meV in the tetragonal phase to 3.7 meV in the orthorhombic phase. The temperature dependence of the intensity around 1.4 meV is plotted in the inset of Fig. 6. The other two excitations at around 7.8 and 16 meV are almost unaffected by the structural transition. The schemes of magnetic excitations for both structure phases are presented in Fig. 7. The measurement at 12 K (not shown, except the low-energy part in the inset of Fig. 6), i.e., in the vicinity of $T_{\text{struc}}^{\text{CePd}_2\text{Al}_2} = 13 \text{ K}$, demonstrates the intermediate stage between phases as the magnetic peak is observed at around 3.4 meV . More detailed description of the influence of structural phase transition on the first excited level of $\text{CePd}_2(\text{Al}, \text{Ga})_2$ compounds can be found below (Sec. III B 5).

Figure 6 contains the low- and high-momentum transfer cuts of both CePd_2Al_2 and LaPd_2Al_2 spectra. The magnetic excitations in the Ce counterpart spectrum can be clearly distinguished from the phonon contributions. The phonon peaks observed at $5, 9, 12,$ and 16.5 meV in the high- Q region [Fig. 6(b)] in both magnetic and nonmagnetic analogs are similar considering the differences in the scattering function. Note that both compounds adopt the orthorhombic crystal structure at $T = 10 \text{ K}$ [13,22]. The phonon energy spectra of CePd_2Al_2 in the tetragonal and orthorhombic phases differ negligibly at $E > 5 \text{ meV}$. Figure 6 leads to several important observations:

- (1) The excitations at $3.7, 7.8,$ and 16 meV in CePd_2Al_2 behave as expected for peaks of magnetic origin.
- (2) The phonon peaks at around $5, 9,$ and 16.5 meV energy transfer, present in both Ce and La analogs, are found at energies very close to those of the magnetic excitations; i.e., the observed peaks in the higher- Q spectrum of CePd_2Al_2 contain both magnetic and phonon contributions.

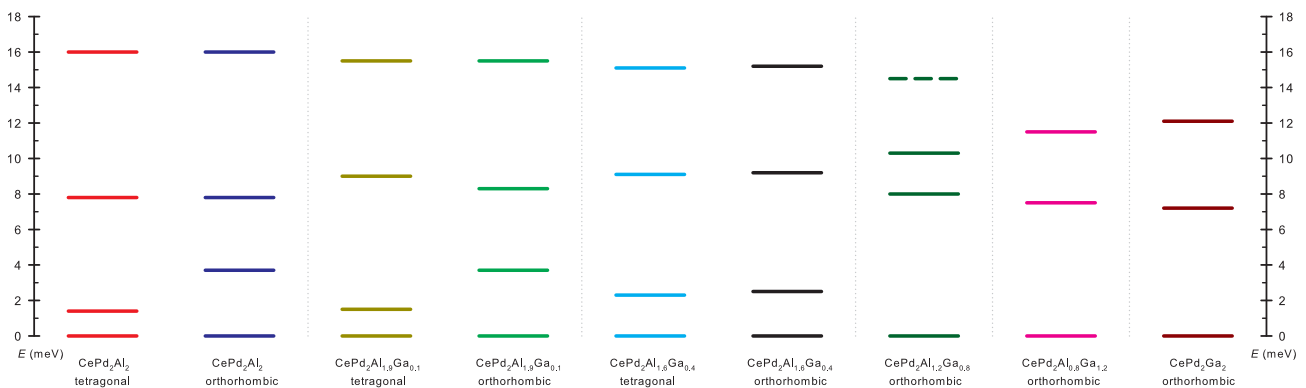


FIG. 7. Schemes of magnetic excitations observed by inelastic neutron scattering in $\text{CePd}_2\text{Al}_{2-x}\text{Ga}_x$ compounds. The excitation energies are taken from Table II. See text and Figs. 5, 6, 8, and 10 for details.

(3) The phonon peak at 12 meV takes place in between other two CF excitation-phonon peaks at 7.8 and 16 meV. This phonon density of states peak was previously observed at around 11 meV by Chapon *et al.* [13] showing a good agreement of both studies. We note the presumably pure lattice nature of this peak; no magnetic contribution is present as seen from comparison of the Ce and La counterpart spectra (Fig. 6).

The inset of Fig. 6 shows the temperature evolution of the 1.4 meV peak. It is absent in IN6 data at low temperatures (actually observed around 3.7 meV in IN4 data), appears at 15 K, stays almost unchanged between 15 K and 40 K, and then gradually decreases with increasing temperature as expected for a peak related to a CF excitation: the first excited CF level is progressively populated (and the ground-state level depopulated) with increasing temperature leading to a decrease of scattering probability. The presence of the peak at -1.4 meV is the consequence of the principle of detailed balance.

3. “Vibron” state in CePd₂Al₂: Comparison with CeCuAl₃

The observation of an additional peak in the energy spectrum of CePd₂Al₂ calls for a comparison with other Ce-based compounds revealing similar phenomena. The energy spectrum of cubic CeAl₂ contains two inelastic features in the paramagnetic regime, while only a single excitation is expected in the cubic symmetry of the crystal field [10]. CeCuAl₃ crystallizing in the tetragonal structure (tetragonal symmetry of the crystal field) reveals three inelastic excitations [14], similarly to CePd₂Al₂. CeCuAl₃ and CePd₂Al₂ represent the only two compounds with noncubic symmetry of the crystal field revealing an additional inelastic non-purely-phononic peak in an energy spectrum, so far. The comparison of physical properties of these two compounds leads to several common characteristics:

(1) The tetragonal crystal structures of CaBe₂Ge₂ type for CePd₂Al₂ [13,22,25] and BaNiSn₃ type for CeCuAl₃ [41] belong to the maximal subgroups of tetragonal space group $I4/mmm$, 139. Moreover, the volume of the elementary unit cell is almost the same for both compounds (192.5 and 194.0 Å³, respectively) [23,41].

(2) A competition between a long-range RKKY interaction and Kondo screening takes place in both compounds leading to a low magnetic ordering temperature and to the exhaustion of a part of the magnetic entropy above the ordering temperature. The estimated Kondo temperature is close to 4 K in both compounds [24,42].

(3) Both compounds order antiferromagnetically below 2.7 K revealing incommensurate amplitude-modulated magnetic structure; see previous section and Ref. [43].

(4) The inelastic neutron scattering (INS) spectra contain three CF-like peaks. All three CF-like excitations display intensities of similar mutual ratios in both compounds. Their characteristic energies are similar. In CeCuAl₃ these excitations are located at 1.3, 9.8, and 20.5 meV [14]. A pure phonon peak in between two higher-energy CF-like peaks is present in the spectra of both compounds. It occurs at around 13.5 meV in CeCuAl₃ [14].

The similarities of the observed energy spectra and also other structural and physical properties of CePd₂Al₂ and

CeCuAl₃ lead us to apply an analogous data analysis to that done for CeCuAl₃ [14] to describe the presence of the additional magnetic peak in the energy spectra.

The observed three magnetic excitations in CePd₂Al₂ cannot be described on the basis of the pure CF model considering the tetragonal (orthorhombic) point symmetry of the crystal field:

$$\widehat{H}_{\text{CEF}}^{\text{tetragonal-Ce}} = B_2^0 \widehat{O}_2^0 + B_4^0 \widehat{O}_4^0 + B_4^4 \widehat{O}_4^4, \quad (1)$$

$$\widehat{H}_{\text{CEF}}^{\text{orthorhombic-Ce}} = B_2^0 \widehat{O}_2^0 + B_2^2 \widehat{O}_2^2 + B_4^0 \widehat{O}_4^0 + B_4^2 \widehat{O}_4^2 + B_4^4 \widehat{O}_4^4. \quad (2)$$

B_m^n are the parameters of the crystal field and \widehat{O}_m^n Stevens' operators representing the cerium 4*f* shell. To explain the present results, we followed the procedure used by Chapon *et al.* [13] and Adroja *et al.* [14] in the case of CeCuAl₃.

The model of CF excitation-phonon interaction developed by Thalmeier and Fulde for cubic CeAl₂ [11], generalized for the tetragonal point group symmetry [14], was used for the fit of the measured INS data:

$$\widehat{H}_{\text{tot}} = \sum_{mn} B_m^n \widehat{O}_m^n + \hbar\omega_0 \left(a_\mu^+ a_\mu + \frac{1}{2} \right) - g_0 \sum_{\mu} (a_\mu + a_\mu^+) \widehat{O}_\mu. \quad (3)$$

The first term stands for the pure CF Hamiltonian [Hamiltonians for the tetragonal and orthorhombic structures shown in Eqs. (1) and (2)]. The second term describes a pure phonon contribution in terms of phonon creation and annihilation operators, and the last part represents the CF excitation-phonon coupling. g_0 and \widehat{O}_μ are the magnetoelastic parameter (proportional to the coupling between CF excitations and phonon density of states) and the CF-phonon operator, respectively.

All data were fitted and CF parameters determined employing the interactive crystal electric field parameter fitting package FOCUS [44] and the FORTRAN program written by Goremychkin [45]. The crystal field is calculated using two methods: Stevens' operator equivalents and 3*j* symbols. Both methods should give exactly the same results and thus the implementation of both provides an easy check of the CF calculation.

In analogy with the data analysis of the previously investigated tetragonal CeCuAl₃ [14], we estimated the CF parameters taking into account only two CF excitations: the low-energy one at 1.4 meV and a high-energy hypothetical one close to the high phonon density of states near 12 meV. The final fit of Eq. (3) to the tetragonal phase data is presented in Fig. 8(b) (dashed line) and refined parameters are listed in Table II. The determined CF parameters are in good agreement with those reported by Chapon *et al.* [13]; the g_0 parameter is however considerably lower. We note that the similar g_0 value of 0.4 meV was found in CeCuAl₃ [14] (using the same fitting program), which exhibits very similar physical properties to those of CePd₂Al₂. As a test, the whole fitting process was repeated with the energies 7.8 and 12 meV supposing that the hypothetical excitation at 12 meV was split into excitations at 1.4 and 16 meV under the influence of phonons. Indeed, we were not able to reproduce the experimental data by the calculated spectrum.

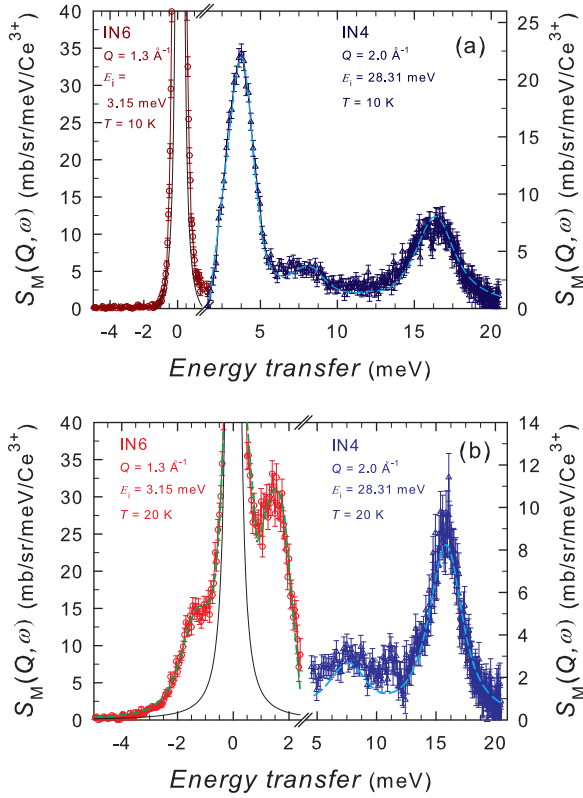


FIG. 8. Constant Q cuts of CePd_2Al_2 (the constant Q cuts were done around center value Q in intervals of 0.5 \AA^{-1}). The LaPd_2Al_2 data were subtracted from the Ce analog for IN4 data; i.e., only the magnetic contributions to the spectra are presented. (a) The energy spectra of CePd_2Al_2 adopting orthorhombic (10 K) and (b) tetragonal (20 K) structures are presented. The presence of the peak at -1.4 meV in (b) is the consequence of the principle of detailed balance. The dashed lines represent the fits with Eq. (3).

We investigated also the energy spectrum of the orthorhombic phase (of CePd_2Al_2). We undertook the whole fitting process starting with energy levels at 3.7 and 12 meV. The refined parameters describing the measured data [see dashed line in Fig. 8(a)] are listed in Table II. Note that this way we

TABLE II. Parameters (B_m^n) and eigenvalues (Δ_i) of the crystal field Hamiltonian describing the CF excitations in $\text{CePd}_2\text{Al}_{2-x}\text{Ga}_x$ compounds [obtained by fits to Eqs. (3) and (2)]; Δ_i values are listed as directly observed in the experimental data in Figs. 8 and 10]. The upper part of the table lists the parameters obtained by fitting the tetragonal ($T = 20 \text{ K}$) and orthorhombic ($T = 10 \text{ K}$ or 5 K) phase data with Eq. (3) (CF-vibron Hamiltonian). $\hbar\omega_0$ and g_0 are fitted phonon energy and magnetoelastic coupling parameter, respectively. The lower part of the table lists the CF eigenvalues and parameters obtained from fits of the orthorhombic data to standard CF Hamiltonian [Eq. (2)]. See text and Figs. 7, 8, and 10 for details.

x	T (K)	Δ_1 (meV)	Δ_2 (meV)	Δ_3 (meV)	B_2^0 (meV)	B_2^2 (meV)	B_4^0 (meV)	B_4^2 (meV)	B_4^4 (meV)	$\hbar\omega_0$ (meV)	g_0 (meV)
0.0	20	1.4(1)	7.8(4)	15.9(3)	0.85(2)		0.023(2)		0.02(1)	8.5(5)	0.35(3)
0.0	10	3.7(3)	7.8(4)	16.0(3)	0.77(2)		0.029(2)		0.01(1)	8.0(5)	0.30(3)
0.1	5	3.7(2)	8.3(3)	15.5(3)	0.71(2)		0.030(2)		0.01(1)	7.6(5)	0.34(3)
0.4	5	2.5(2)	9.2(4)	15.2(3)	0.75(2)		0.026(2)		0.01(1)	8.1(5)	0.34(3)
0.8	10	8.0(2)	11.0(3)	14.5(4)	0.14(1)		0.035(2)		0.015(4)	12.7(5)	0.43(3)
0.8	10	8.0(2)	11.0(3)		0.35(2)	0.100(5)	-0.009(1)	0.114(1)	0.040(4)		
1.2	10	7.5(2)	11.5(4)		0.38(1)	0.253(4)	-0.009(1)	0.110(1)	0.060(3)		
2.0	10	7.2(2)	12.1(2)		0.33(1)	0.472(4)	-0.009(1)	0.111(1)	0.055(3)		

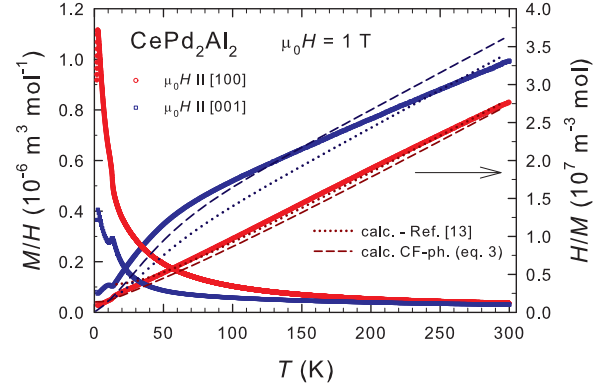


FIG. 9. Temperature dependence of magnetization measured on CePd_2Al_2 single crystal (data taken from Ref. [24]). Magnetic field was applied along principal tetragonal crystallographic directions. The calculated curves are given: dotted line represents the calculated H/M from tetragonal CF parameters given in Ref. [13]. The dashed line stays for CF parameters obtained by fitting the measured INS spectra with Eq. (3) (CF excitation-phonon interaction). More details in text and in Table II. The observed anomalies at the low-temperature part of the figure can be identified with structural and magnetic phase transitions in CePd_2Al_2 .

fitted the INS data of the orthorhombic phase with tetragonal CF parameters. Nevertheless, such a fit should serve as the first estimation of the magnetoelastic parameter g_0 in the compound (also taking into account relatively small difference between crystal structures of phases). The generalization of Thalmeier-Fulde model to describe also the orthorhombic symmetry of crystal field is essential for the correct data treatment and represents a challenge for theory.

4. Susceptibility measurement on a CePd_2Al_2 single crystal

We compared the obtained CF parameters with our magnetic susceptibility data measured on a CePd_2Al_2 single crystal (see also Ref. [24]). The calculated temperature dependencies of susceptibility are plotted in Fig. 9: the dotted line represents the calculated H/M from tetragonal CF parameters given in Ref. [13]. The dashed line stands for CF parameters

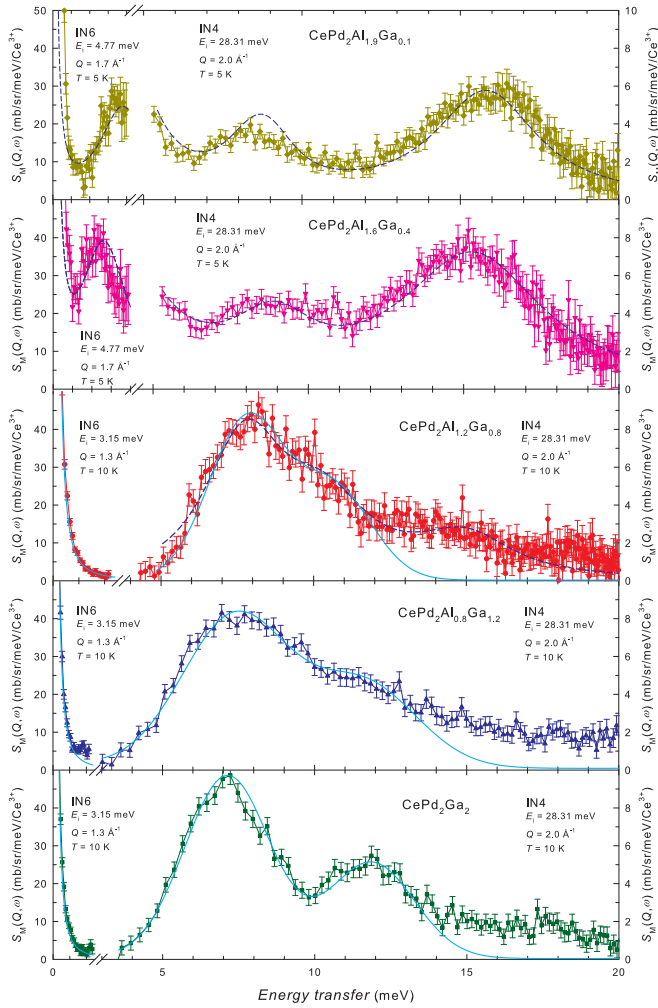


FIG. 10. Constant Q cuts of $\text{CePd}_2\text{Al}_{2-x}\text{Ga}_x$ compounds crystallizing in orthorhombic structure (the constant Q cuts were done around center value Q in intervals of 0.5 and 1 \AA^{-1} for IN6 and IN4 data, respectively). The magnetic contributions were derived by subtraction of the $\text{LaPd}_2(\text{Al,Ga})_2$ data from the Ce counterparts (higher-energy part of figure) as described in the text. The dashed line represents the fit with Eq. (3) taking three magnetic excitations, while only two excitations were considered fitting the data with Eq. (2) (full curve). The fitted CF parameters are listed in Table II.

obtained by fitting the measured INS spectra with Eq. (3) (CF excitation-phonon interaction). Comparing calculated curves with measured single-crystal data, better agreement is obtained for CF parameters determined from our INS data with Eq. (3). However, we note that neither of the two sets of CF parameters is able to fully describe the measured susceptibility as we were not able to incorporate the magnetoelastic coupling into the calculation of magnetic susceptibility.

5. Crystal field excitations in $\text{CePd}_2\text{Al}_{1.9}\text{Ga}_{0.1}$ and $\text{CePd}_2\text{Al}_{1.6}\text{Ga}_{0.4}$

To follow the evolution of the crystal field excitations and of a possible presence of an additional magnetic excitation in the $\text{CePd}_2(\text{Al,Ga})_2$ system, inelastic neutron scattering experiments with the IN6 and IN4 spectrometers were performed

also for several compounds with different Al-Ga content. The measurements were done at several temperatures for both the tetragonal and the orthorhombic phase.

$\text{CePd}_2\text{Al}_{1.9}\text{Ga}_{0.1}$ exhibits an energy spectrum quite similar to that of the parent CePd_2Al_2 , including both magnetic and phonon contributions. We observe three magnetic excitations with similar intensities at similar energies for both compounds—in the case of $\text{CePd}_2\text{Al}_{1.9}\text{Ga}_{0.1}$ at 1.5 (3.7), 8.2 (7.9), and 16.0 (15.6) meV for tetragonal (orthorhombic) phase. See Figs. 7 and 10 and Table II. The inelastic spectra were fitted with Eq. (3) leading to CF parameters and parameter g_0 very similar to parent CePd_2Al_2 ; see Table II.

Here, we should discuss the evolution of CF energy levels depending on the degree of orthorhombic distortion of the tetragonal structure (see Fig. 1). The structural phase transition (or, better to say orthorhombic distortion) has a significant influence on the first excited CF level as demonstrated in Fig. 11. The excitation energy remains almost the same at temperatures down to 12 K, where $\text{CePd}_2\text{Al}_{1.9}\text{Ga}_{0.1}$ adopts the tetragonal structure [22]. With further cooling we observe the shift of this level to higher energies. The shift is continuous in a large temperature interval (down to base temperature 1.5 K).

The lattice parameters in parent CePd_2Al_2 (see Fig. 1 in Ref. [13]) and $\text{CePd}_2\text{Al}_{1.9}\text{Ga}_{0.1}$ exhibit only very weak temperature dependence in the tetragonal phase above T_{struc} , undergo an abrupt change on a relatively short temperature interval around T_{struc} , and then develop smoothly with further cooling. Similar behavior shows also the first magnetic excitation in these compounds which energy remains unchanged in the tetragonal phase and increases rapidly just below the structural transition as illustrated in Fig. 11. The energy of the remaining two magnetic excitations do not show any significant temperature changes, so it is just only the first excitation which clearly reflects the temperature evolution of structural parameters around and below the T_{struc} .

Further substitution of Al by Ga does not change the energy spectrum significantly as found for $\text{CePd}_2\text{Al}_{1.6}\text{Ga}_{0.4}$. We still observe three clear magnetic peaks in the spectrum as well as a phonon peak around 11.5 meV, similarly as in CePd_2Al_2 and $\text{CePd}_2\text{Al}_{1.9}\text{Ga}_{0.1}$. However, the CF levels are shifted in energy compared to former compounds. We repeated the whole fitting process with Eq. (3) leading to the results listed in Table II and plotted in Fig. 10. Contrary to CePd_2Al_2 and $\text{CePd}_2\text{Al}_{1.9}\text{Ga}_{0.1}$, the energy of the lowest magnetic excitation does not change significantly when cooling down to the lowest temperature (see Fig. 7 and Table II). This observation is well in agreement with the development of lattice parameters as observed by x-ray diffraction which shows that the orthorhombic distortion in $\text{CePd}_2\text{Al}_{1.6}\text{Ga}_{0.4}$ is rather small and can be considered just as a microstrain [22].

6. Crystal field excitations in CePd_2Ga_2 and $\text{CePd}_2\text{Al}_{2-x}\text{Ga}_x$ compounds with $x \geq 0.8$

Let us now turn to the opposite end of the series. The inelastic spectra of CePd_2Ga_2 (see Fig. 10) show only two clear CF peaks located around 7.2 and 12.1 meV. There is no evidence for an additional third excitation as observed for the Al-rich compounds. We note that the higher excitation around

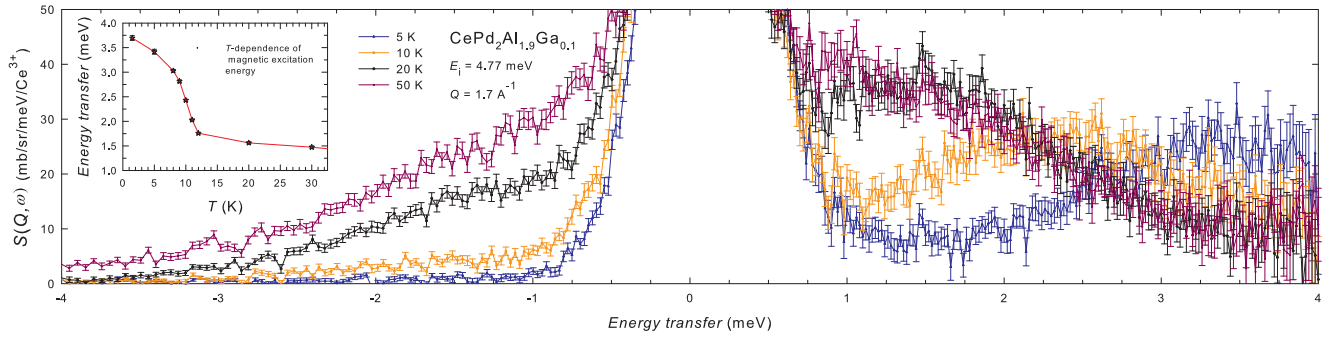


FIG. 11. Constant Q cuts of energy spectra measured on $\text{CePd}_2\text{Al}_{1.9}\text{Ga}_{0.1}$ at different temperatures. The constant Q cuts were done around center value Q in intervals of 0.5 \AA^{-1} . The temperature evolution of magnetic peak maximum is traced out and plotted in the inset.

12 meV is close to the hypothetical energy level anticipated when applying Eq. (3) to the CePd_2Al_2 case. The spectrum can be well fitted by standard CF model yielding the CF parameters given in Table II. The corresponding fit is drawn in Fig. 10. We note that the determined CF parameters need to be confronted with measurements of other physical properties on single crystals. The precise CF parameter values cannot be fully determined based on INS data only as the point group symmetry of the Ce site is lower than cubic. Unfortunately, at

the present time we are not able to prepare appropriate single crystals of CePd_2Ga_2 or Al-Ga substitutions.

$\text{CePd}_2\text{Al}_{0.8}\text{Ga}_{1.2}$ exhibits an energy spectrum similar to that of CePd_2Ga_2 ; just the two CF peaks are broader and closer to each other. The broadness of peaks can be understood taking into account the influence of Al-Ga substitution on solid solution properties (the covalent radii of Al and Ga have nearly the same value of 121 pm and 122 pm, respectively). The spectrum can be again well fitted by the standard CF

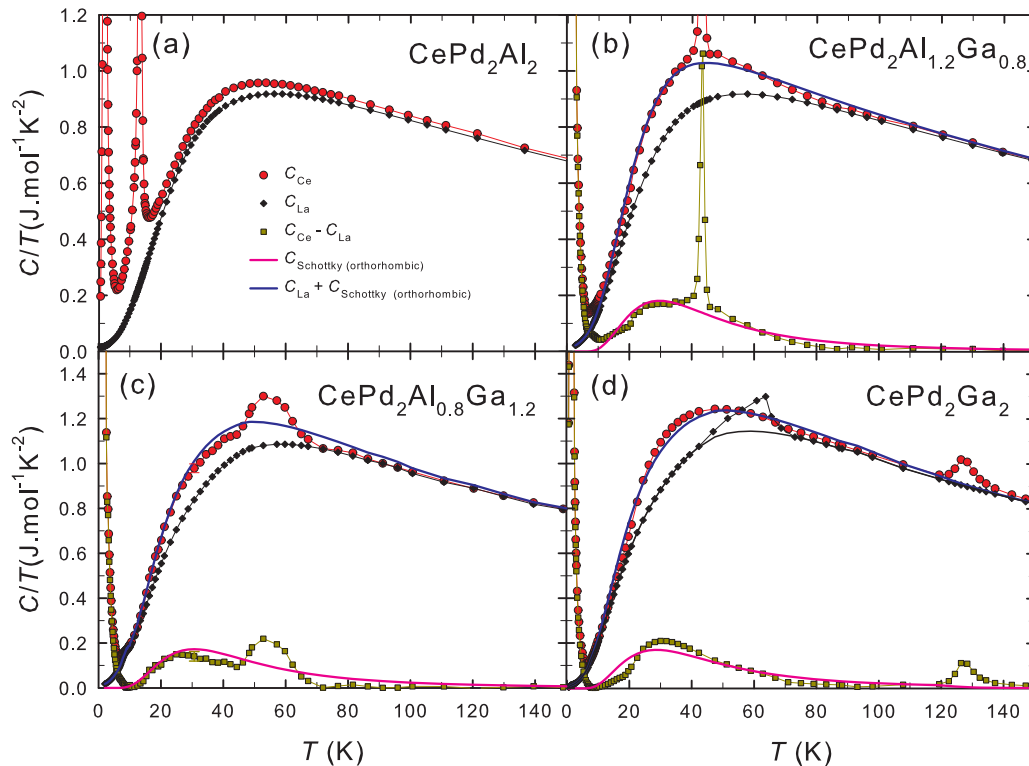


FIG. 12. Specific heat of $\text{CePd}_2\text{Al}_{2-x}\text{Ga}_x$ and nonmagnetic analogs $\text{LaPd}_2\text{Al}_{2-x}\text{Ga}_x$, together with their difference and Schottky specific heat calculated from the energies determined by INS experiments. Schottky contributions were calculated based on three doubly degenerated levels with energies listed in Table II. The structural phase transitions in $\text{CePd}_2\text{Al}_{2-x}\text{Ga}_x$ and LaPd_2Ga_2 are clearly pronounced in the specific-heat data. As the magnetophonon interaction has a strong impact on both magnetic and lattice contributions of specific heat in CePd_2Al_2 , the Schottky contribution was not calculated. The anomaly on LaPd_2Ga_2 data makes it difficult to estimate the magnetic contribution to the specific heat of the Ce analog; therefore, we used a smooth (black) curve displayed in the panel (d) for the subtraction of electron and phonon contributions from the total specific heat of CePd_2Ga_2 . For illustration, the error bar at $\approx 30 \text{ K}$ in panel (c) corresponds to 2% error of the specific-heat measurement.

model; the resulting CF parameters given in Table II are close to those of CePd_2Ga_2 .

Finally, the spectra of $\text{CePd}_2\text{Al}_{1.2}\text{Ga}_{0.8}$ can be, to some extent, interpreted in both ways—either using Eq. (3) or within the standard CF Hamiltonian [Eq. (2)]. First, we fit the spectra taking two standard CF levels at 8 and 11 meV. The calculated inelastic response is drawn as a full line in Fig. 10 and the corresponding parameters are listed in Table II. The enhanced intensity observed at around 14.5 meV might be connected with the influence of Al-Ga substitution on solid solution properties, which is mirrored also in the enhanced broadness of the observed peaks. A non-negligible signal is observed at high energies also for other Al-Ga substitutions; see Fig. 10. Another possibility of how to view the data is to consider three excitations at around 8, 11, and 14.5 meV and describe the spectra using Eq. (3) as for CePd_2Al_2 . The data are fitted taking a hypothetical state at around 12 meV. The interaction with phonons then leads to formation of states at around 11 and 14.5 meV. The refined parameters are listed in Table II and the fit to the data is presented as a dashed line in Fig. 10. We note that the B_2^0 parameter is significantly different compared to CePd_2Al_2 while B_4^0 and B_4^4 are quite similar in both compounds. The magnetoelastic parameter, g_0 , is slightly higher at the same time.

The inelastic neutron spectra of CePd_2Ga_2 , $\text{CePd}_2\text{Al}_{0.8}\text{Ga}_{1.2}$, and $\text{CePd}_2\text{Al}_{1.2}\text{Ga}_{0.8}$ measured at higher temperatures in the tetragonal phase of these compounds (not shown) reveal almost identical energy level schemes to those in the orthorhombic phase. This is in contrast to CePd_2Al_2 and $\text{CePd}_2\text{Al}_{1.9}\text{Ga}_{0.1}$ where a substantial change for the first excited level occurs. There are two factors making the quantitative analysis of the spectra complicated: (i) the broadening of the features and their mutual vicinity and (ii) the structural transition temperatures for the Ga-rich compounds are rather high [23]; i.e., the low-lying energy levels are substantially occupied at temperatures at which the compounds adopt the tetragonal structure.

The determined energy level schemes for compounds with high Ga content (Fig. 7) were also confronted with the specific-heat data. In general, the measurement of the specific heat corroborates well the energy schemes as determined from neutron spectra. The experimental magnetic specific heat is compared to the Schottky contribution calculated using (orthorhombic phase) energies listed in Table II (only two excited doublets taken into account). The agreement between the data and calculations is quite remarkable for all the compounds; see Fig. 12. As the excitation energies in $\text{CePd}_2\text{Al}_{2-x}\text{Ga}_x$ with $x \geq 0.8$ are almost the same regardless the crystal structure, the agreement is very good also at higher temperatures in the tetragonal phase. The structural and magnetic phase transitions reveal themselves as anomalies in the specific heat at temperatures corresponding to those determined by our magnetization and electrical resistivity studies [23,24]. Note the sharp anomaly for $\text{CePd}_2\text{Al}_{1.2}\text{Ga}_{0.8}$ compared to rather broad ones in compounds with higher Ga content. The details of the development of the structural transition depending on the Ga concentration will be a subject of our separate paper [22]. We do not present the Schottky calculation for Al-rich compounds where also the phonons are affected by the electron-phonon interaction and

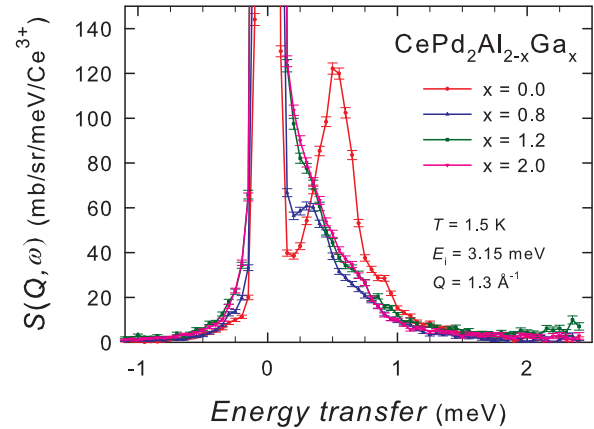


FIG. 13. Constant Q cuts of $\text{CePd}_2\text{Al}_{2-x}\text{Ga}_x$ data measured at temperatures $< T_N$ (the constant Q cuts were done around center value Q in interval of 0.5 \AA^{-1}). The shift of the low-energy excitation (the splitting of doublet ground state) with the Ga content to lower energies is observed.

the determination of magnetic part of the specific heat is rather ambiguous; only measured specific-heat data are given for CePd_2Al_2 and LaPd_2Al_2 in Fig. 12.

7. Splitting of the ground-state doublet in $\text{CePd}_2(\text{Al,Ga})_2$ compounds

We also investigated the energy spectra of the compounds below their Néel temperature T_N ($2.2 \text{ K} \leq T_N \leq 2.7 \text{ K}$ for all Al-Ga concentrations). We observe the splitting of the doublet ground state as presented in Fig. 13. The low-energy magnetic peak is clearly visible at around 0.5 meV in CePd_2Al_2 , at almost the same energy (0.48 meV) in $\text{CePd}_2\text{Al}_{1.9}\text{Ga}_{0.1}$ (not shown for lucidity), around 0.35 meV in $\text{CePd}_2\text{Al}_{1.6}\text{Ga}_{0.4}$ (not shown), and around 0.3 meV in $\text{CePd}_2\text{Al}_{1.2}\text{Ga}_{0.8}$. For compounds with higher Ga content, the splitting shifts to even lower excitation energies which might be related to the change of electronic properties and magnetic structures with Al-Ga substitution in the $\text{CePd}_2(\text{Al,Ga})_2$ series. Indeed, the bulk studies show slightly different magnetic behavior [23] and also our diffraction experiments revealed quite different magnetic structures in the parent compounds. See also Sec. III B 1.

8. Discussion: Energy spectra in $\text{CePd}_2(\text{Al,Ga})_2$ and relation to structural properties

The present neutron scattering study was intended to corroborate the hypothesis [13] about the relation between the CF excitation-phonon interaction and the stability of the tetragonal structure in CePd_2Al_2 and Al-Ga substituted compounds. Previous structure investigations revealed relatively small orthorhombic distortion in CePd_2Al_2 [13] in contrast to much larger distortion in CePd_2Ga_2 [21,22] (see Fig. 1 to relate both cases). The change between these two types of structural behavior within the $\text{CePd}_2\text{Al}_x\text{Ga}_{2-x}$ series is reflected by the concentration dependence of the electrical resistivity in this series [23] which shows well pronounced transitions at relatively high temperatures at the Ga-rich end, whereas the transition is much less pronounced and occurs at relatively low temperatures for the Al-rich end of the

series. Our present neutron scattering experiment revealed clear correspondence between these structural changes and concentration development of observed energy spectra. We verified the presence of three magnetic excitations in CePd₂Al₂ in agreement with Chapon *et al.* [13] and observed similar spectra with three magnetic excitations for Al-rich compounds ($x < 0.8$). The additional peak is not observed for compounds with high Ga content.

Furthermore, we observe a strong temperature dependence of the first magnetic excitation at the Al-rich end of the series (see Fig. 7). Its energy increases considerably when undergoing the distortion from tetragonal to orthorhombic phase. Such strong temperature dependence is clearly observed in CePd₂Al₂ and CePd₂Al_{1.9}Ga_{0.1}. The next studied composition, CePd₂Al_{1.6}Ga_{0.4}, already does not show such significant changes when cooling down to the lowest temperature of 1.5 K (see Fig. 7). This observation corresponds to the development of lattice parameters observed by x-ray diffraction [22] which shows that the orthorhombic distortion in CePd₂Al_{1.6}Ga_{0.4} is rather small and can be considered just as a microstrain as mentioned already above in Sec. III B 5. We can thus state that the energy of the first magnetic excitation for CePd₂Al_xGa_{2-x} with $x \leq 0.4$ directly reflects the stage of the orthorhombic distortion.

An open question is related to the necessary prerequisites for the formation of the vibron states. The high phonon density of states at around 12 meV is clearly found in all CePd₂(Al,Ga)₂ compounds and their La counterparts. Hypothetical existence of a CF excitation around the same energy was considered as a prerequisite for the CF-phonon interaction and the vibron state formation in both CePd₂Al₂ [13] and CeCuAl₃ [14]. However, the CF excitation at 12 meV is clearly observed also in CePd₂Ga₂ where the vibron state (additional magnetic peak) is not observed. The nature of the CF state (wave functions) and the phonon type at this energy might play a role and deserve further investigation mainly using neutron scattering on single crystals. The role of an atomic disorder on certain sites also cannot be completely neglected as it might affect the local CF potential acting on the individual Ce ions.

IV. CONCLUSIONS

The investigation of CePd₂Al_{2-x}Ga_x compounds by means of neutron scattering techniques revealed their magnetic structures and energy schemes.

The magnetic structure of CePd₂Al₂ is described by an incommensurate propagation vector $\vec{k} = (\delta_x, \frac{1}{2} + \delta_y, 0)$ with $\delta_x = 0.06$ and $\delta_y = 0.04$. The magnetic moments on Ce atoms are arranged antiferromagnetically within the orthorhombic planes and point along the direction close to the orthorhombic [100]. The derived magnetic moment reaches the maximum value of $1.5 \mu_B/\text{Ce}^{3+}$. CePd₂Ga₂ reveals the magnetic structure composed of two components. The first of them is described by the propagation vector $\vec{k}_1 = (\frac{1}{2}, \frac{1}{2}, 0)$, while the second one propagates with $\vec{k}_2 = (0, \frac{1}{2}, 0)$. The magnetic moments of both components are collinear to the orthorhombic [100]. Total magnetic moment varies depending on the mutual phase of the magnetic-moment components on each Ce

site. The magnetic structure of substituted CePd₂Al_{2-x}Ga_x compounds is described also by propagation vectors \vec{k}_1 and \vec{k}_2 , except a magnetic structure of CePd₂Al_{1.9}Ga_{0.1}. Observed magnetic reflections in CePd₂Al_{1.9}Ga_{0.1} can be described by propagation vectors \vec{k} and \vec{k}_1 , which stands this compound on the border between pure CePd₂Al₂ and the rest of the series.

CePd₂Al_{2-x}Ga_x compounds with $x \leq 0.4$ show three magnetic excitations, while only two crystal field excitations are expected for cerium-based material. The additional magnetic peak can be well described within the Thalmeier-Fulde model of CF-phonon coupling generalized for the tetragonal point symmetry. The Ga-rich compounds show the standard two CF excitations. CePd₂Al_{1.2}Ga_{0.8} exhibits an energy spectrum staying on the border between the Al-rich and Ga-rich parts of the series. This concentration development of energy spectra corresponds well to structural properties and the occurrence of the orthorhombic distortion within the series. The orthorhombic distortion has a significant impact on the energy of lowest magnetic excitation in Al-rich compounds. Furthermore, we provide a clear relation between the development of structural properties and observed energy spectra in the studied series.

ACKNOWLEDGMENTS

The preparation and characterization of (Ce,La)Pd₂(Al,Ga)₂ samples were performed at MLTL (<http://mltl.eu>), which is supported within the program of Czech Research Infrastructures (Project No. LM2011025). We acknowledge Institute Laue-Langevin (ILL), Grenoble, France, for the allocation of time on the IN6, IN4, and D1B instruments and technical services. The complete sets of the experimental data can be found in Refs. [30–32]. The work was supported within the program of Large Infrastructures for Research, Experimental Development, and Innovation (Project No. LM2015050) and Research Project No. LG14037 financed by the Ministry of Education, Youth, and Sports, Czech Republic.

APPENDIX

The orthorhombic structure parameters and determined propagation vectors $\vec{k}_1 = (\frac{1}{2}, \frac{1}{2}, 0)$ and $\vec{k}_2 = (0, \frac{1}{2}, 0)$ were used to perform thorough symmetry analysis. In Secs. III A 2 and III A 3 the details on magnetic structure determination are given. We have used representation analysis employing the BasRep program from the FullProf package [27]. In parallel we investigated possible magnetic structure as maximal magnetic subgroups of paramagnetic space group $Cmme1'$ using the program MaxMagn [33]. The analysis revealed that there are only two maximal magnetic subgroups of $Cmme1'$ described by the propagation vector \vec{k}_1 : monoclinic P_a2 (3) and triclinic $P_5\bar{1}$ (2). The magnetic moments in the P_a2 group, using the setting $(2a, 2b, c)$, are constrained to the basal plane for Ce on monoclinic crystallographic sites $(0, \frac{1}{8}, z_{\text{Ce}})$, whereas moments on sites $(0, \frac{3}{8}, -z_{\text{Ce}})$ point along the orthorhombic c axis. The triclinic $P_5\bar{1}$ group allows any direction of magnetic moments in space.

The investigation of maximal magnetic subgroups compatible with the propagation vector \vec{k}_2 in $Cmme1'$ leads to 8 magnetic space groups with orthorhombic symmetry: P_bmmn

(59), $P_c b c m$ (57), $P_a c c a$ (54), $P_c m n a$ (53), $P_a m n a$ (53), $P_a m m a$ (51), $P_a b a n$ (50), and $P_a c c m$ (49). These groups can be divided into four families according to the arrangements of the magnetic moments. The groups $P_b m m n$ (59) and $P_a m m a$ (51) imply two different Ce atomic sites $(0, \frac{1}{8}, z_{Ce})$ and $(0, \frac{3}{8}, -z_{Ce})$, the first with magnetic moments along the a axis and the second with zero moments. The same atomic sites are found also in groups $P_c b c m$ (57) and $P_a m n a$ (53), but the magnetic moments point along the c axis and along the b axis, respectively. The third family consists of groups $P_a c c a$ (54) and $P_a b a n$ (50) with magnetic moments constrained in the bc plane. Finally, the groups $P_c m n a$ (53) and $P_a c c m$ (49) constrain the magnetic moments along the a axis.

The magnetic peaks corresponding to \vec{k}_2 are the strongest in $CePd_2Ga_2$. For the incommensurate structure of $CePd_2Al_2$ the propagation vector is $\vec{k} = \vec{k}_2 + (\delta_x, \delta_y, 0)$ with $\delta_x = 0.06$ and $\delta_y = 0.04$; therefore the magnetic structures are mainly described by \vec{k}_2 . In the case of $CePd_2Ga_2$ none of the maximal subgroups of $Cmme1'$ compatible with \vec{k}_2 (listed above) gives an adequate refinement of the corresponding peaks. The data refinement points out magnetic moments to be arranged within the basal plane. However constraining the magnetic moment to the ab plane the maximal symmetry of the \vec{k}_2 component of the diffraction pattern is monoclinic with magnetic group $P_a 2/c$. Considering the \vec{k}_1 component the total symmetry reduces to $P_5 1$.

-
- [1] F. Steglich, J. Aarts, C. D. Bredl, W. Lieke, D. Meschede, W. Franz, and H. Schäfer, *Phys. Rev. Lett.* **43**, 1892 (1979).
- [2] B. Bellarbi, A. Benoit, D. Jaccard, J. M. Mignot, and H. F. Braun, *Phys. Rev. B* **30**, 1182 (1984).
- [3] T. Endstra, G. J. Nieuwenhuys, and J. A. Mydosh, *Phys. Rev. B* **48**, 9595 (1993).
- [4] F. M. Grosche, S. R. Julian, N. D. Mather, and G. G. Lonzarich, *Physica B* **223-224**, 50 (1996).
- [5] R. Movshovich, T. Graf, D. Mandrus, J. D. Thompson, J. L. Smith, and Z. Fisk, *Phys. Rev. B* **53**, 8241 (1996).
- [6] D. Jaccard, K. Behnia, and J. Sierro, *Phys. Lett. A* **163**, 475 (1992).
- [7] H. Yamaoka, Y. Zekko, A. Kotani, I. Jarrige, N. Tsujii, J. F. Lin, J. Mizuki, H. Abe, H. Kitazawa, N. Hiraoka, H. Ishii, and K. D. Tsuei, *Phys. Rev. B* **86**, 235131 (2012).
- [8] T. Toliński, K. Synoradzki, M. Koterlyn, G. Koterlyn, and R. Yasnitskii, *J. Alloys Compd.* **580**, 512 (2013).
- [9] C. Ammarguella, M. Escorne, A. Mauger, E. Beaupaire, M. F. Ravet, G. Krill, F. Lapierre, P. Haen, and C. Godart, *Phys. Stat. Sol. B* **143**, 159 (1987).
- [10] M. Loewenhaupt, B. D. Rainford, and F. Steglich, *Phys. Rev. Lett.* **42**, 1709 (1979).
- [11] P. Thalmeier and P. Fulde, *Phys. Rev. Lett.* **49**, 1588 (1982).
- [12] M. Loewenhaupt, W. Reichardt, R. Pynn, and E. Lindley, *J. Magn. Magn. Mater.* **63-64**, 73 (1987).
- [13] L. C. Chapon, E. A. Goremychkin, R. Osborn, B. D. Rainford, and S. Short, *Physica B* **378-380**, 819 (2006).
- [14] D. T. Adroja, A. del Moral, C. de la Fuente, A. Fraile, E. A. Goremychkin, J. W. Taylor, A. D. Hillier, and F. Fernandez-Alonso, *Phys. Rev. Lett.* **108**, 216402 (2012).
- [15] E. A. Goremychkin, I. Natkaniec, E. Mühle, and O. D. Chistyakov, *J. Magn. Magn. Mater.* **81**, 63 (1989).
- [16] M. Ruminy, E. Pomjakushina, K. Iida, K. Kamazawa, D. T. Adroja, U. Stuhr, and T. Fennell, *Phys. Rev. B* **94**, 024430 (2016).
- [17] M. Ruminy, L. Bovo, E. Pomjakushina, M. K. Haas, U. Stuhr, A. Cervellino, R. J. Cava, M. Kenzelmann, and T. Fennell, *Phys. Rev. B* **93**, 144407 (2016).
- [18] W. P. Beyermann, M. F. Hundley, P. C. Canfield, C. Godart, M. Selsane, Z. Fisk, J. L. Smith, and J. D. Thompson, *Physica B* **171**, 373 (1991).
- [19] T. Takabatake, T. Tanaka, Y. Bando, H. Fujii, N. Takeda, M. Ishikawa, and I. Oguro, *Physica B* **230-232**, 223 (1997).
- [20] A. Dommann, F. Hullier, H. R. Ott, and V. Gramlich, *J. Less-Common Met.* **110**, 331 (1985).
- [21] J. Kitagawa and M. Ishikawa, *J. Phys. Soc. Jpn.* **68**, 2380 (1999).
- [22] P. Doležal, M. Klicpera, J. Prchal, and P. Javorský (unpublished).
- [23] M. Klicpera, P. Javorský, and A. Hoser, *J. Alloys Compd.* **596**, 167 (2014).
- [24] M. Klicpera, P. Doležal, J. Prokleška, J. Prchal, and P. Javorský, *J. Alloys Compd.* **639**, 51 (2015).
- [25] A. Tursina, E. Khamitcaeva, A. Gribanov, D. Gnida, and D. Kaczorowski, *Inorg. Chem.* **54**, 3439 (2015).
- [26] M. Klicpera, J. Pásztorová, and P. Javorský, *Supercond. Sci. Technol.* **27**, 085001 (2014).
- [27] J. Rodríguez-Carvajal, *Physica B* **192**, 55 (1993).
- [28] LAMP, the Large Array Manipulation Program.
- [29] D. Richard, M. Ferrand, and G. J. Kearley, *J. Neutron Research* **4**, 33 (1996).
- [30] M. Klicpera, P. Javorský, J. Pásztorová, and I. Puente Orench, Magnetic structure investigation in $CePd_2Al_2$ compound, Institut Laue-Langevin (ILL), doi:10.5291/ILL-DATA.5-31-2304.
- [31] M. Klicpera, P. Doležal, P. Javorský, M. M. Koza, and S. Rols, Vibron states investigation in $CePd_2(Al, Ga)_2$ compounds, Institut Laue-Langevin (ILL), doi:10.5291/ILL-DATA.7-01-400.
- [32] M. Klicpera, P. Doležal, P. Javorský, H. Mutka, and S. Rols, Vibron states in $CePd_2Al_{1.9}Ga_{0.1}$ and $CePd_2Al_{1.6}Ga_{0.4}$ compounds, Institut Laue-Langevin (ILL), doi:10.5291/ILL-DATA.7-01-442.
- [33] J. M. Perez-Mato, S. V. Gallego, E. S. Tasci, L. Elcoro, G. de la Flor, and M. I. Aroyo, *Annu. Rev. Mater. Res.* **45**, 217 (2015).
- [34] J. Rodríguez-Carvajal and F. Bourée, *EPJ Web Conf.* **22**, 00010 (2012).
- [35] R. A. Steeman, E. Frikkee, R. B. Helmholdt, A. A. Menovsky, J. van den Berg, G. J. Nieuwenhuys, and J. A. Mydosh, *Solid State Commun.* **66**, 103 (1988).
- [36] B. Fåk, E. Ressouche, G. Knebel, J. Flouquet, and P. Lejay, *Solid State Commun.* **115**, 407 (2000).
- [37] R. Feyerherm, B. Becker, M. F. Collins, J. Mydosh, G. J. Nieuwenhuys, and S. Ramakrishnan, *Physica B* **241-243**, 643 (1998).
- [38] B. H. Grier, J. M. Lawrence, V. Murgai, and R. D. Parks, *Phys. Rev. B* **29**, 2664 (1984).

- [39] S. Raymond, P. Haen, R. Calemczuk, S. Kambe, B. Fåk, P. Lejay, T. Fukuhara, and J. Flouquet, *J. Phys.: Condens. Matter* **11**, 5547 (1999).
- [40] G. Knopp, A. Loidl, K. Knorr, L. Pawlak, M. Duczmal, R. Caspary, U. Gottwick, H. Spille, F. Steglich, and A. P. Murani, *Z. Phys. B: Condens. Matter* **77**, 95 (1989).
- [41] M. Klicpera, P. Javorský, P. Čermák, A. Rudajevová, S. Daniš, T. Brunátová, and I. Císařová, *Intermetallics* **46**, 126 (2014).
- [42] P. Javorský and M. Klicpera, *J. Magn. Magn. Mater.* **342**, 152 (2013).
- [43] M. Klicpera, P. Javorský, P. Čermák, A. Schneidewind, B. Ouladdiaf, and M. Diviš, *Phys. Rev. B* **91**, 224419 (2015).
- [44] P. Fabi, Tech. Rep. RAL-TR-95-023, Didcot, United Kingdom, 1995.
- [45] E. G. Goremychkin (unpublished).